High-spin states in La136 and possible structure change in the N=79 region

H. Nishibata, R. Leguillon, A. Odahara, T. Shimoda, C. M. Petrache, Y. Ito, J. Takatsu, K. Tajiri, N. Hamatani, R. Yokoyama, et al.

High-spin states in ^{136}La and possible structure change in the $N = 79$ region

H. Nishibata,[1] R. Leguillon,[2,3,*] A. Odahara,[1] T. Shimoda,[1] C. M. Petrache,[2,3] Y. Ito,[1] J. Takatsu,[1] K. Tajiri,[1] N. Hamatani,[4] R. Yokoyama,[5] E. Ideguchi,[4] H. Watanabe,[6] Y. Wakabayashi,[6] K. Yoshinaga,[7] T. Suzuki,[4] S. Nishimura,[6] D. Beaumel,[3] G. Lehaut,[8] D. Guinet,[8] P. Desesquelles,[2] D. Curien,[9,10] K. Higashiyama,[11] and N. Yoshinaga[12]

[1]*Department of Physics, Osaka University, Osaka 560-0043, Japan*
[2]*Centre de Sciences Nucléaires et de Sciences de la Matière, Université Paris-Sud and CNRS/IN2P3, 91405 Orsay, France*
[3]*Institut de Physique Nucléaire d'Orsay (IPNO), CNRS/IN2P3, 91405 Orsay, France*
[4]*Research Center for Nuclear Physics (RCNP), Osaka University, Ibaraki, Osaka 567-0047, Japan*
[5]*Center for Nuclear Study (CNS), University of Tokyo, Wako, Saitama 351-0198, Japan*
[6]*RIKEN, Wako, Saitama 351-0198, Japan*
[7]*Tokyo University of Science, Noda, Chiba 278-8510, Japan*
[8]*Institut de Physique Nucléaire de Lyon (IPNL), 69622 Villeurbanne, France*
[9]*Université de Strasbourg, IPHC, 23 rue du Loess 67037 Strasbourg, France*
[10]*CNRS, UMR7178, 67037 Strasbourg, France*
[11]*Department of Physics, Chiba Institute of Technology, Narashino, Chiba 275-0023, Japan*
[12]*Department of Physics, Saitama University, Saitama 338-8570, Japan*

(Received 15 January 2015; revised manuscript received 31 March 2015; published 7 May 2015)

High-spin states in the odd-odd nucleus ^{136}La, which is located close to the β-stability line, have been investigated in the radioactive-beam-induced fusion-evaporation reaction ^{124}Sn(^{17}N,5n). The use of the radioactive beam enabled a highly sensitive and successful search for a new isomer [14^+, $T_{1/2} = 187(27)$ ns] in ^{136}La. In the $A = 130$–140 mass region, no such long-lived isomer has been observed at high spin in odd-odd nuclei. The ^{136}La level scheme was revised, incorporating the 14^+ isomer and six new levels. The results were compared with pair-truncated shell model (PTSM) calculations which successfully explain the level structure of the $\pi h_{11/2} \otimes \nu h_{11/2}^{-1}$ bands in ^{132}La and ^{134}La. The isomerism of the 14^+ state was investigated also by a collective model, the cranked Nilsson-Strutinsky (CNS) model, which explains various high-spin structures in the medium-heavy mass region. It is suggested that a new type of collective structure is induced in the PTSM model by the increase of the number of $\pi g_{7/2}$ pairs, and/or in the CNS model by the configuration change associated with the shape change in ^{136}La.

DOI: 10.1103/PhysRevC.91.054305 PACS number(s): 25.60.−t, 23.35.+g, 23.20.Lv, 27.60.+j

I. INTRODUCTION

In the odd-odd transitional nuclei with $A = 130$–140, both the valence protons and neutrons are in the same shell between the 50 and 82 magic numbers. The proton and neutron Fermi surfaces are located below and above the $h_{11/2}$ orbit, respectively. Therefore, a naive configuration of the high-spin states is $\pi h_{11/2} \otimes \nu h_{11/2}^{-1}$. With increasing rotational frequency, the interaction between the valence protons and the core induces rotational alignment, and as a result a prolate deformation is driven, whereas the neutron holes tend to induce an oblate deformation. Because of competition between these deformations, various types of shapes are expected [1]. The rotation axis can also be oriented along different axes depending on the configuration [2]. In La isotopes, exotic phenomena such as signature splitting [3], signature inversion [4], and chiral band [5] have been observed and they were ascribed to triaxial deformation.

In ^{136}La, a typical $\pi h_{11/2} \otimes \nu h_{11/2}^{-1}$ band has been observed [6–8]. However, the proposed level schemes are not in agreement with each other: Fig. 1 shows the partial level schemes of ^{136}La proposed by three groups of Cybulska *et al.* based on the ^{128}Te(^{11}B,3n) reaction at 4.4 MeV/u [6], Zhu *et al.* on the ^{130}Te(^{11}B,5n) reaction at 5.5 MeV/u [7], and Bhattacharjee *et al.* on the same reaction as the latter but at 4.7 MeV/u [8]. Note that the band head, which is located 0.865 MeV above the 114 ms isomer [9], is taken as a reference. The spin-parity assignment for the reference level is 8^+, (9^+), or 9^+, according to the 8^+, (8^+), or 7^- assignment for the 114 ms isomer, respectively. The level structure is significantly different above the 12^+ or 13^+ levels. In this situation it is rather difficult to discuss the nuclear structure. The difference may be due to unobserved isomers. The level scheme should be investigated in dedicated experiments which are sensitive to possible isomers.

We have performed an experiment, placing an emphasis on the high-spin states and isomers in La isotopes. Our specific feature is the use of the radioactive nuclear beam ^{17}N ($T_{1/2} = 4.2$ s [10]) to achieve a high sensitivity for the high-spin isomers. Figure 2 shows the estimated population distributions of the ^{136}La states after fusion-evaporation reactions, displayed in a spin vs. excitation-energy plane for the ^{130}Te(^{11}B,5n)^{136}La reaction at 4.7 MeV/u used in Ref. [8] (upper panel) and the ^{124}Sn(^{17}N,5n)^{136}La reaction at 5.2 MeV/u used in the present work (lower panel). The populations were estimated by the CASCADE code [11]. It

[*]Present address: Advanced Science Research Center, Japan Atomic Energy Agency, Tokai, Ibaraki 319-1195, Japan.

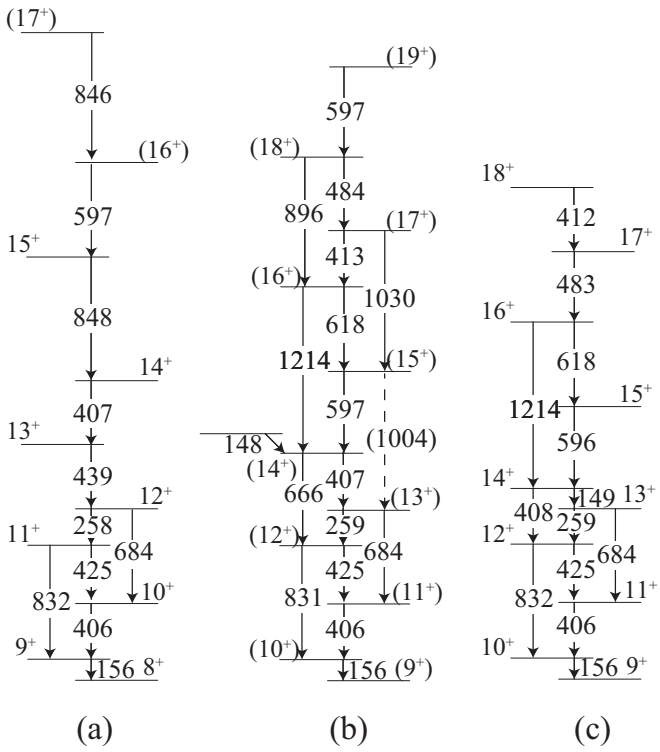

FIG. 1. Partial level schemes of ^{136}La proposed by (a) Ref. [6], (b) Ref. [7], and (c) Ref. [8]. The levels above the $\pi h_{11/2} \otimes \nu h^{-1}_{11/2}$ band head are displayed.

is expected that the higher mass and the higher energy of the projectile bring in higher angular momentum and lead to higher excitation energy in the residual nucleus. In Fig. 2, it is indeed clearly seen that higher spin and higher excitation-energy states are populated in the ^{124}Sn(^{17}N,5n)^{136}La reaction than in the ^{130}Te(^{11}B,5n)^{136}La reaction. This will

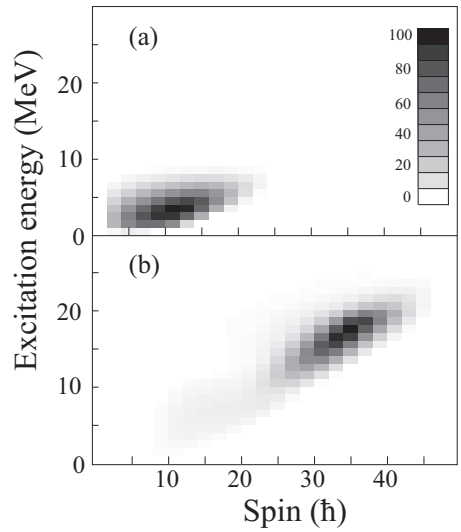

FIG. 2. Estimated relative population distributions in a spin vs. excitation-energy plane for (a) ^{130}Te(^{11}B,5n)^{136}La at 4.7 MeV/u, as in the previous work [8], and (b) ^{124}Sn(^{17}N,5n)^{136}La at 5.2 MeV/u, as in the present work.

enable high-S/N measurements for the high-spin states. The ^{124}Sn(^{17}N,5n)^{136}La reaction at 5.2 MeV/u is uniquely optimum among various reactions to populate the high-spin states in ^{136}La with the highest-S/N ratio. Another advantage of the (^{17}N,5n) reaction is that the beam particle can be detected on the event-by-event basis. It makes the measurement highly sensitive to the high-spin isomers and helps in reducing the background significantly.

In the present work, the high-spin states in ^{136}La and ^{135}La were populated in the above-mentioned reaction. This paper reports the results of ^{136}La and discusses the level structure in ^{136}La. The results of ^{135}La have been reported recently in a separate publication [12].

II. EXPERIMENT

The experiment was performed at the Research Center for Nuclear Physics (RCNP), Osaka University. The high-spin states in ^{136}La were populated by bombarding a ^{124}Sn target (20 mg/cm^2 thick, 97.5% enriched) with ^{17}N beam. The ^{17}N beam with an energy of 5.2 MeV/u was produced by the ^{9}Be(^{18}O, ^{17}N)^{10}B reaction at 9.3 MeV/u and transported to the secondary beam-line [13,14], which is shown in Fig. 3. The ^{18}O primary beam was injected with a tilt angle of $\sim$1.8° at the primary target to reduce the contaminants in the ^{17}N secondary beam. The repetition period of the ^{18}O primary beam was 148 ns, and the beam reference signal for the TOF measurement was provided in every other period so as to allow firm identification of the secondary particles in a ΔE-TOF spectrum.

The magnetic rigidity selection was optimized for ^{17}N^{7+} with an acceptance of $\Delta(B\rho)/B\rho = 3.5\%$ at the dispersive

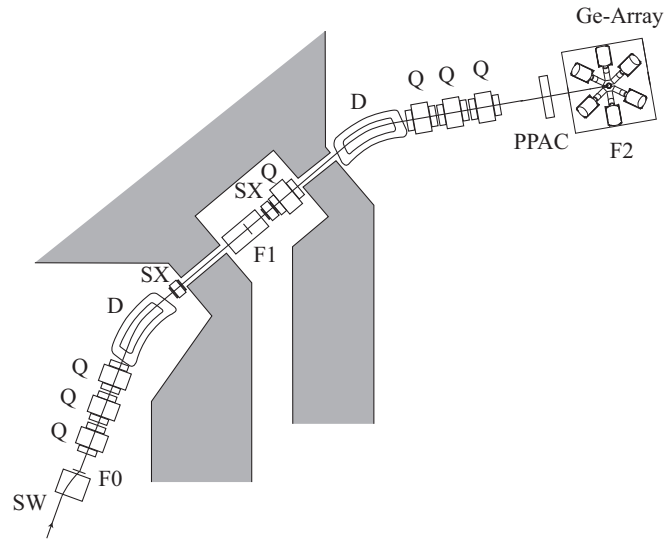

FIG. 3. Schematic layout of the secondary beam-line at RCNP [13,14]. The dipole, quadrupole, and sextupole magnets are denoted by D, Q, and SX, respectively. The beam swinger magnet (SW) makes the primary beam tilted at the production target F0. The reaction products are angular-focused at the dispersive focal plane F1 and achromatic-focused at F2, where the beam-particle detector (PPAC) and the Ge array are placed.

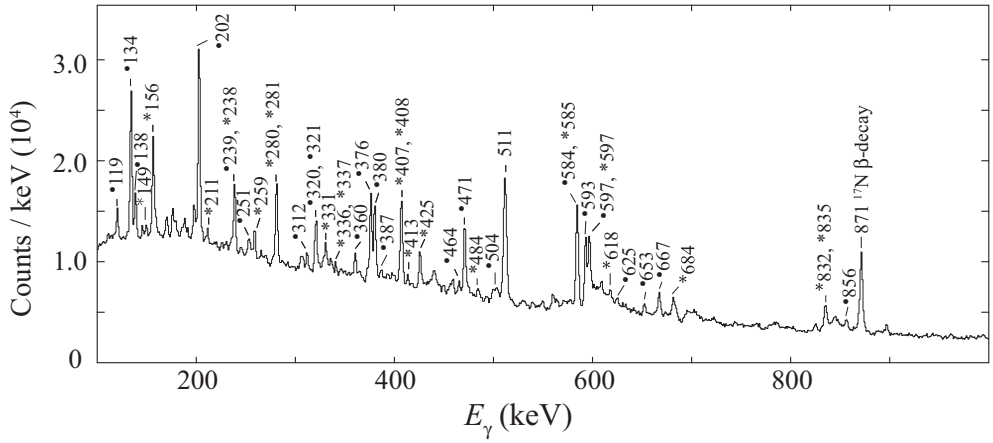

FIG. 4. Total γ-γ projection spectrum with the time window of $\pm$800 ns. The peaks labeled with closed circles and asterisks are originated from the known γ rays associated with ^{135}La and ^{136}La, respectively. The numbers are the γ-ray energies in keV.

focal plane F1. The ^{17}N beam was achromatic-focused into a spot size of $\sim$22 mm (FWHM) in diameter on the secondary ^{124}Sn target at F2. The intensity of the secondary ^{17}N beam was 1.2×10^5 pps with the primary ^{18}O beam intensity of 1.5 pμA. The purity of the ^{17}N beam was approximately 90%. The major beam contaminants were $^{18}O^{6+}$, $^{18}O^{7+}$, $^{15}C^{6+}$, and $^{12}C^{5+}$. They did not cause any significant effect to the experiment.

The γ rays from the fusion-evaporation reaction products were measured by a detector array consisting of 12 high-purity germanium (Ge) detectors surrounding the ^{124}Sn target. Eight of the detectors were used with BGO anti-Compton shields (ACSs) to enable high-S/N γ-ray measurements and to reduce the Compton cross-talk events between Ge detectors. The detectors were placed at 30° (four Ge with ACSs), 90° (four Ge), and 150° (four Ge with ACSs) with respect to the beam direction. All the Ge detectors were placed at a distance of 140 mm from the ^{124}Sn target. The total detection efficiency was determined to be 3.2% for 1.3-MeV γ ray. The beam particles were detected by the parallel plate avalanche counter (PPAC), placed at 1.5 m upstream from the ^{124}Sn target. The PPAC-γ coincidence measurement enabled low-background measurements and highly sensitive detection of the isomers. The total counts of PPAC-γ and γ-γ coincidence events were 6.8×10^7 and 2.4×10^6, respectively, in the accumulation time of 86 h.

III. RESULTS

A. Principle of analysis

The total projection spectrum of γ-γ coincidence data is shown in Fig. 4. The coincidence measurement with a time window of $\pm$800 ns was performed in order to cover all the delayed-γ rays associated with isomers, if any. Because of the largest and the second largest cross sections of the ^{124}Sn(^{17}N,6n)^{135}La and ^{124}Sn(^{17}N,5n)^{136}La reactions, respectively, most of the strong peaks in Fig. 4 are due to the known γ rays in ^{135}La [12,15] and ^{136}La [6–9]. Many other small peaks are also seen in the spectrum. Some of them may be the candidates for unknown γ rays in ^{136}La.

The newly established level scheme of ^{136}La was constructed by examining the detailed γ-γ coincidence relations, the γ-ray intensities, and the timing information between two γ rays, as well as that between a γ ray and the associated beam particle (PPAC signal). The construction of the level scheme was made in four steps:

(1) First the levels associated with intense γ rays were assigned by examining the γ-ray coincidence relations.

(2) The isomers were searched for by referring to the time difference between the beam and the γ rays. If any isomers, the delayed component should be observed in the time difference spectrum between the beam and the γ rays emitted from the levels which are located below the isomers.

(3) The location of the isomer in the level scheme was assigned by examining the coincidence relation between "delayed" γ rays and "prompt" γ rays. Here we name the γ rays detected in time windows of $\pm$50 ns and 100-800 ns, with respect to the PPAC timing, "prompt" and "delayed" γ rays, respectively. Figure 5 schematically shows the essence of the method. The events are plotted in a two-dimensional matrix of (energy of prompt γ ray) vs. (energy of delayed γ ray), which is called $E_{\text{prompt-}\gamma} - E_{\text{delayed-}\gamma}$ matrix. The prompt and delayed events are selected by gating on the time difference between the beam and the γ rays, as shown in the time spectrum displayed in the inset of Fig. 5. Since the first γ ray, γ_1, is emitted promptly and the cascade γ rays, γ_2 and γ_3, are delayed, a large number of coincidence events should be observed as shown by the thick lines and closed circles in the matrix, and the former and the latter two γ rays should be enhanced in the projection spectrum of $E_{\text{prompt-}\gamma}$ and $E_{\text{delayed-}\gamma}$, respectively, as schematically shown in the figure. In such a way we could unambiguously identify the isomeric levels and the γ rays above and below the isomer. Therefore, we could locate the isomers in the level scheme.

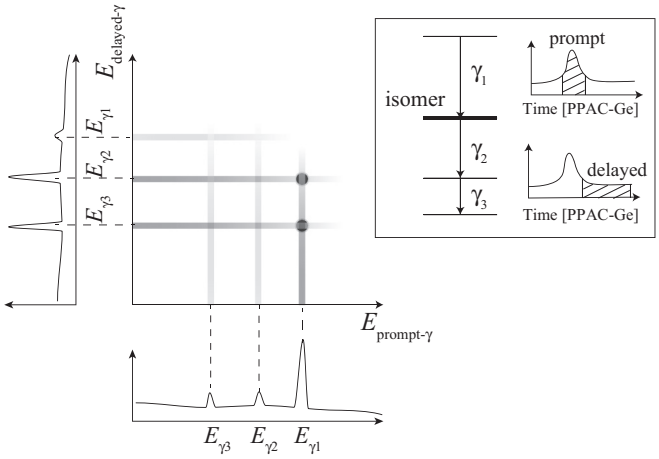

FIG. 5. Schematic two dimensional matrix of (energy of prompt γ ray) vs. (energy of delayed γ ray), i.e., $E_{\text{prompt-}\gamma} - E_{\text{delayed-}\gamma}$ matrix, assuming an illustrative level scheme in the inset, and projection spectra. The time gates for the prompt and delayed coincidence are schematically shown in the inset.

(4) Weak γ rays above the isomers were clearly identified by using the $E_{\text{prompt-}\gamma} - E_{\text{delayed-}\gamma}$ matrix.

B. Search for isomers

As the first step of analysis, the sum of coincidence spectra gated by the known ^{136}La γ rays (156, 281, 407, and 425 keV) was obtained with the time window of $\pm$800 ns as shown in Fig. 6. These four γ rays were assigned to originate from ^{136}La by the previous works [6–8]. In the present work, the 149-, 259-, 280-, 336-, 408-, 585-, 597-, 618-, 678-, and 684-keV γ-ray peaks were confirmed as the cascade γ rays leading to these four intense transitions.

As the second step, the isomers were searched for by using time difference spectra between the beam and the respective γ rays as discussed above. Examples of time spectra with respect to the beam are shown in Fig. 7. A long tail is observed in the time spectrum gated by the 281-keV γ ray in Fig. 7(a), whereas the time spectrum gated by the 618-keV γ ray shown in Fig. 7(b) has only a prompt component. This means that at least one isomer should exist between the two levels de-excited by the 281- or 618-keV γ rays. The same examinations were performed for all 14 γ rays seen in Fig. 6. It was found that

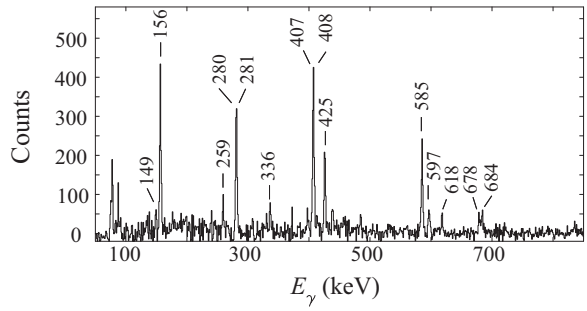

FIG. 6. Sum of coincidence spectra gated by the intense 156-, 281-, 407-, and 425-keV γ rays with a time window of $\pm$800 ns.

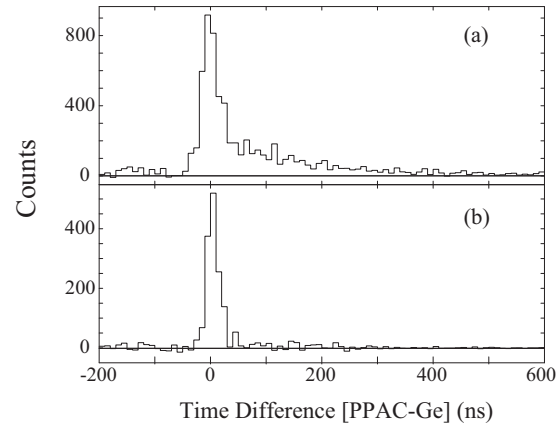

FIG. 7. Time difference spectra between the beam (PPAC) and the γ rays gated by (a) 281-keV and (b) 618-keV γ rays.

the time spectra for the γ rays of 149, 156, 259, 281, 407, 408, 425, 585, and 684 keV have delayed components, whereas those for 280, 336, 597, 618, and 678 keV have only prompt components.

In the third step, the analysis using the $E_{\text{prompt-}\gamma} - E_{\text{delayed-}\gamma}$ matrix was carried out to assign the isomeric state and to establish the level scheme. Figure 8 shows the sum of coincidence spectra gated by the intense γ rays (156, 281, 407, 425, and 585 keV) associated with the low-lying levels in ^{136}La. The upper and lower panels show delayed and prompt γ-ray spectra with delayed-delayed and delayed-prompt γ-γ coincidences, respectively. The γ rays of 149, 156, 259, 281, 407, 408, 425, 585, and 684 keV are clearly observed in the upper panel, whereas in the lower panel they are significantly suppressed and many peaks, which are not noticed in the upper panel, appear. The peaks with asterisk are newly found γ rays in the present work. From the detailed analyses based on the $E_{\text{prompt-}\gamma} - E_{\text{delayed-}\gamma}$ matrix, the observed γ rays were classified into three groups: (i) transitions below the isomer (149, 156, 259, 281, 407, 408, 425, 585, and 684 keV), (ii) transitions above the isomer (238, 306, 331, 337, 398, 413,

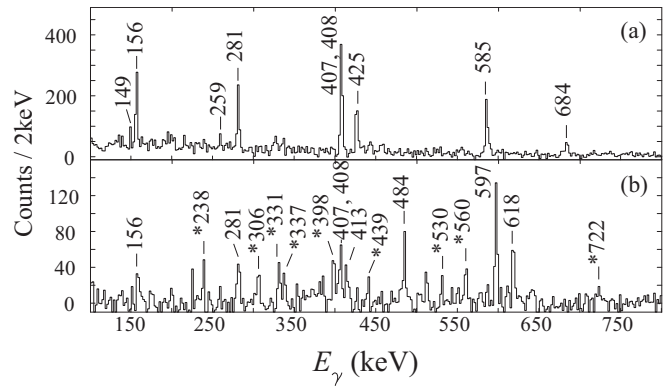

FIG. 8. Sum of coincidence spectra gated by the 156-, 281-, 407-, 425-, and 585-keV γ rays (a) with coincidence between the delayed-γ components and the delayed-γ components, (b) with coincidence between the delayed-γ and the prompt-γ components. The γ-ray peaks labeled with asterisks are newly found in the present work.

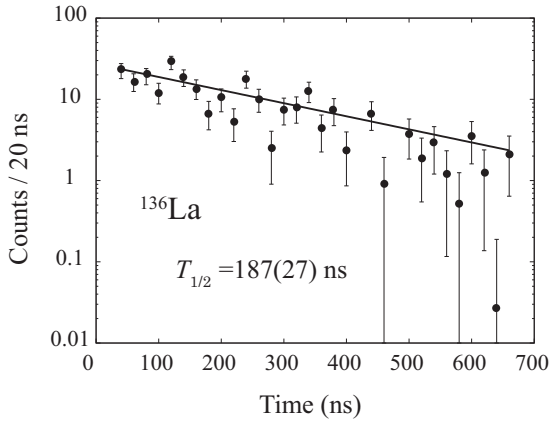

FIG. 9. Time spectrum of the newly found isomer at $\widetilde{E}_x = 2.261$ MeV in ^{136}La. The solid line is the result of least-square fitting with an exponential function.

439, 484, 530, 560, 597, 618, and 722 keV), and (iii) transitions bypassing the isomer (280, 336, and 678 keV).

As shown in Fig. 1, the level scheme up to the level de-excited by the 259-keV γ ray is in good agreement with the previous three works [6–9]. The present work also confirms the part of the previous level scheme associated with the 156-, 259-, 281-, 407-, 425-, 585-, and 684-keV transitions in group (i). A level was placed at 2.261 MeV above the 114 ms isomer based on the energy consistency between 148.6(5)+258.5(3) = 407.1(6) keV and 407.8(4) keV, as well as the coincidence relations. The level scheme up to this level is consistent with Ref. [8]. Hereafter the excitation energy of the levels is expressed in the reduced form, scaled from the 114 ms isomer, so that the above-mentioned level energy is shown as $\widetilde{E}_x = 2.261$ MeV.

The fact that the 413-, 484-, 597-, and 618-keV γ rays are grouped in (ii) suggests that the $\widetilde{E}_x = 2.261$ MeV level is the isomer. This was confirmed by the half-life measurement for the $\widetilde{E}_x = 2.261$ MeV level. The time spectrum of the new isomer is shown in Fig. 9. The half-life of 187(27) ns was obtained from the sum of the time spectra of 16 combinations between the γ rays in group (ii) (413, 484, 597, and 618 keV) and those in group (i) (407, 425, 585, and 684 keV). The time resolution of the Ge detectors (30 ns typical) has little influence to the result.

C. Level scheme

The level scheme of ^{136}La above the $\widetilde{E}_x = 2.261$ MeV isomer was revised in the present work, as shown in Fig. 10. The transitions and levels associated with asterisks were observed for the first time.

The spin-parity assignments and level placements were performed as follows. The level pattern of the $\pi h_{11/2} \otimes \nu h^{-1}_{11/2}$ band in ^{136}La is very similar to those in ^{130}La [16], ^{132}La [17], and ^{134}La [18]. Therefore, from the systematics, we reasonably propose the spin-parity of the band members as (9^+) ($\widetilde{E}_x$ = 0.865 MeV) up to (13^+) ($\widetilde{E}_x = 2.112$ MeV). Note that the isomerism of the $\widetilde{E}_x = 2.261$ MeV level can be explained by the negative-parity assignment such as 14^-. However, we adopt the same (14^+) assignment as Bhattacharjee *et al.* [8] who has clarified the $M1$ and $E2$ characters of the 149- and 408-keV transitions, respectively, in the measurements of linear polarization and angular correlations [8]. From the decay pattern, the levels at $\widetilde{E}_x = 2.858$, 3.476, 3.888, and 4.372 MeV are most likely the same band members as the $\widetilde{E}_x = 2.261$ MeV level. This results in the assignment of (15^+), (16^+), (17^+), and (18^+) for the $\widetilde{E}_x = 2.858$, 3.476, 3.888, and 4.372 MeV levels, respectively. The $E1$ and $M1$ characters of the 585- and 281-keV transitions [8] lead to spin-parity of (8^-) and (7^-) for the $\widetilde{E}_x = 0.281$ and 0 MeV levels, respectively, whereas in Ref. [9] (7^-) and (8^+) assignments are adopted for these levels, respectively. We adopt the latest assignments by Bhattacharjee *et al.* [8] up to the (16^+) level at $\widetilde{E}_x = 3.476$ MeV.

In Fig. 8(b) nine new γ rays of 238, 306, 331, 337, 398, 439, 530, 560, and 722 keV in group (ii) are observed. A new level at $\widetilde{E}_x = 4.770$ MeV was proposed based on the fact that a γ-ray peak of 398 keV was observed with high intensity in the γ-γ coincidence spectrum gated by the 484-keV γ ray. New levels ($\widetilde{E}_x = 4.679$ MeV and 5.209 MeV) and their depopulating γ rays were proposed based on consistency of the energy sums of the γ rays: 306.2(2)+529.7(3) = 835.9(4) and 397.5(2)+439.0(1) = 836.5(2). The order of the transitions was determined from the γ-ray intensity. A new level at $\widetilde{E}_x = 4.611$ MeV was also proposed based on the intensity and energy consistency between 4610.6(3) [238.2(1)+4372.4(3)] keV and 4610.5(6) [722.2(4)+3888.3(4)] keV. Another new level was proposed at $\widetilde{E}_x = 4.035$ MeV based on the energy consistency of 897.0(3) [559.8(2)+337.2(2)] keV and 896.8(5) [4372.4(3)−3475.6(4)] keV. A reversed order of the cascade transitions of 559.8 keV and 337.2 keV is also possible. In this case the reduced excitation energy of the new level will be 3.8128(4) MeV. A new level at $\widetilde{E}_x = 4.941$ MeV de-excited by the 331-keV γ ray was also tentatively proposed.

The spins and parities of the side-band members built on the $\widetilde{E}_x = 2.321$ MeV level were determined from the $E1$ character of the 678 keV transition [8]. The 1030-keV and 892-keV transitions displayed with dashed arrows in Fig. 10 were observed in the total projection spectrum, but their coincidence relations could not be confirmed due to low statistics. They were placed according to the previous reports [7,8].

In order to evaluate the relative intensities of γ transitions, an efficiency-weighted γ-γ matrix was constructed at first using all 12 Ge detectors, then the relative intensities of γ rays were estimated by the peak counts in the projection spectrum gated by the most intense 281-keV γ ray. The effects of the angular correlation were not taken into account. The detailed results concerning the γ transitions are listed in Table I.

IV. DISCUSSION

A. Systematic comparison with neighboring nuclei

The level energies of the $\pi h_{11/2} \otimes \nu h^{-1}_{11/2}$ bands are compared for the $Z = 57$ isotopes and $N = 79$ isotones in Figs. 11 and 12, respectively. Figure 11 shows the comparison of the experimental level energies up to 17^+ in ^{130}La [16], ^{132}La [17], ^{134}La [18], and ^{136}La of the present work. The

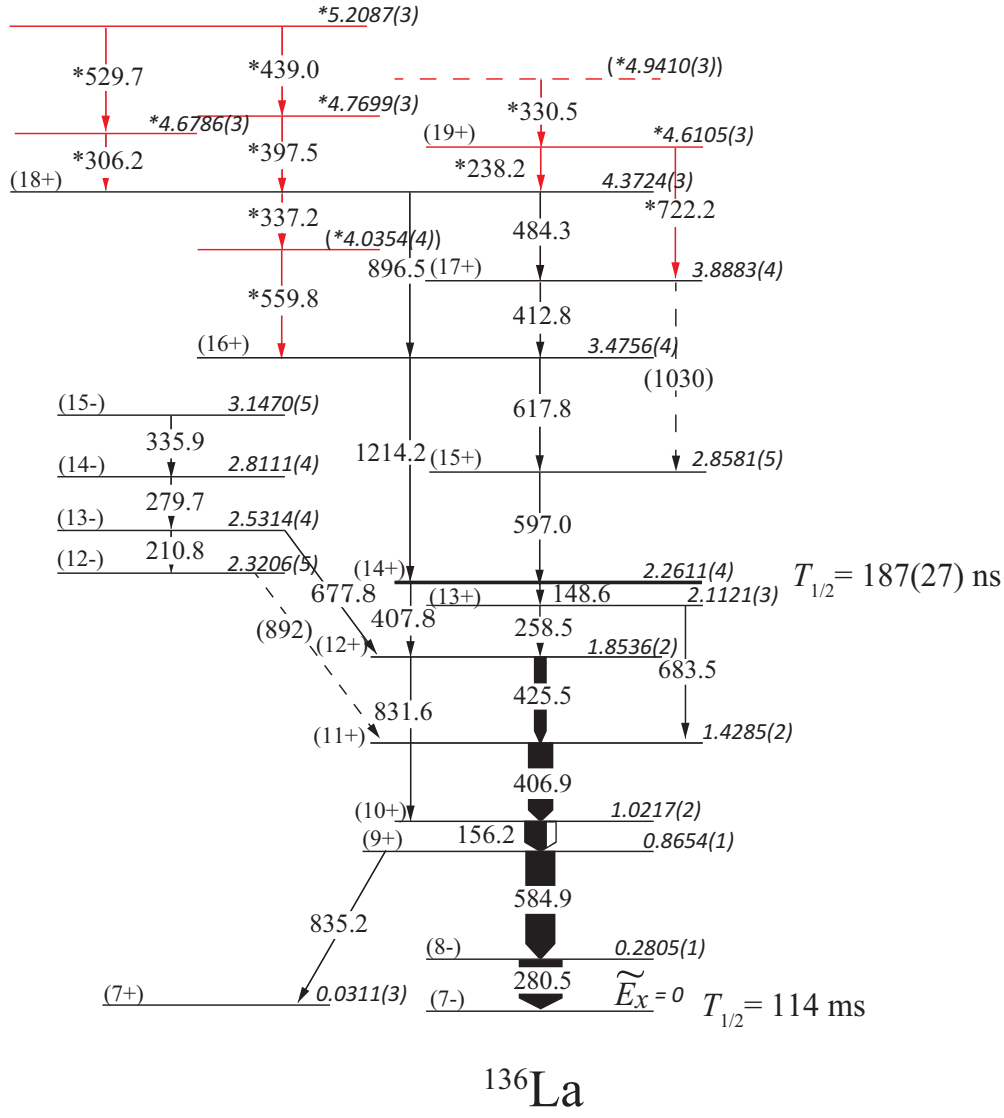

FIG. 10. (Color online) Partial level scheme of ^{136}La established in the present work. The excitation energy is shown in the reduced form of $\widetilde{E}_x$, in which the excitation energy is scaled from that of the 114 ms isomer. The transitions and levels associated with asterisks were observed for the first time and are newly proposed, respectively. Tentative transitions and levels are displayed with dashed arrows and lines, respectively. The arrows denoting the γ transitions schematically illustrate the intensities of the observed γ transitions (black) and of the calculated internal conversion (white).

level energies are shown relative to the 9^+ level, which is the $\pi h_{11/2} \otimes \nu h^{-1}_{11/2}$ band head. It is clearly seen that the level energies up to 12^+ smoothly increase with increasing neutron number. However, those of the 13^+ through 17^+ levels decrease in ^{136}La. In particular the 14^+ level shows an abrupt decrease. Figure 12 shows the comparison between the $N = 79$ isotones, ^{134}Cs [20], ^{136}La of the present work, ^{138}Pr [21], and ^{140}Pm [22]. It is seen that the energies of the levels up to 12^+ are almost the same in these nuclei, whereas the levels above 13^+ show clear variation as a function of the proton number.

In order to get more insight of the 14^+ isomer, Table II compares the experimental partial half-lives with the Weisskopf estimates for the two transitions de-exciting the 14^+ isomer. It is found that both the $M1(14^+ \rightarrow 13^+)$ and $E2(14^+ \rightarrow 12^+)$ transitions are hindered to a large extent. The level-energy deviation from the systematics and the significant hindrance of the transition probability strongly suggest that in ^{136}La the nuclear structures of the 14^+ and higher spin levels are rather different from those of the lower spins levels.

B. Comparison with pair-truncated shell model prediction

The experimental levels in the $\pi h_{11/2} \otimes \nu h^{-1}_{11/2}$ band of ^{136}La are compared with the pair-truncated shell model (PTSM) calculations [23] which are successful in explaining the level energies and γ-transition probabilities of the $\pi h_{11/2} \otimes \nu h^{-1}_{11/2}$ band members in ^{132}La and ^{134}La [24]. The PTSM truncates the shell-model subspace constructed in terms of collective pairs with angular momentum zero (S pair), two

TABLE I. Observed γ rays in ^{136}La. The excitation energies of the initial and final states are shown respectively in the reduced form of $\widetilde{E}$i and $\widetilde{E}_{\rm f}$, which are scaled from the 114 ms isomer. The γ-ray intensities $I_{\gamma+ce}$ including calculated internal conversion intensities by using the coefficients in Ref. [19] are shown relative to that of the 281-keV γ ray.

E_γ (keV)	$I_{\gamma+ce}$(%)	$\widetilde{E}_{\rm i}$ (MeV)	$\widetilde{E}_{\rm f}$ (MeV)	$I_{\rm i}^{\pi}$	$I_{\rm f}^{\pi}$	E_γ (keV)	$I_{\gamma+ce}$(%)	$\widetilde{E}_{\rm i}$ (MeV)	$\widetilde{E}_{\rm f}$ (MeV)	$I_{\rm i}^{\pi}$	$I_{\rm f}^{\pi}$
148.6(5)	5(2)	2.2611(4)	2.1121(3)	(14^+)	(13^+)	439.0(1)	2.3(9)	5.2087(3)	4.7699(3)		
156.21(8)	59(5)	1.0217(2)	0.8654(1)	(10^+)	(9^+)	484.3(2)	5(2)	4.3724(3)	3.8883(4)	(18^+)	(17^+)
210.8(3)	6(4)	2.5314(4)	2.3206(5)	(13^-)	(12^-)	529.7(3)	2.1(9)	5.2087(3)	4.6786(3)		
238.2(1)	2.1(8)	4.6105(3)	4.3724(3)	(19^+)	(18^+)	559.8(2)	4(1)	(4.0354(4))	3.4756(4)		(16^+)
258.5(3)	7(2)	2.1121(3)	1.8536(2)	(13^+)	(12^+)	584.9(1)	58(8)	0.8654(1)	0.2805(1)	(9^+)	(8^-)
279.7(2)	8(3)	2.8111(4)	2.5314(4)	(14^-)	(13^-)	597.0(4)	15(3)	2.8581(5)	2.2611(4)	(15^+)	(14^+)
280.52(6)	100	0.2805(1)	0.0	(8^-)	(7^-)	617.8(1)	7(2)	3.4756(4)	2.8581(5)	(16^+)	(15^+)
306.2(2)	2.2(8)	4.6786(3)	4.3724(3)		(18^+)	677.8(3)	4(3)	2.5314(4)	1.8536(2)	(13^-)	(12^+)
330.5(1)	4(1)	(4.9410(3))	4.6105(3)		(19^+)	683.5(3)	13(3)	2.1121(3)	1.4285(2)	(13^+)	(11^+)
335.9(3)	9(3)	3.1470(5)	2.8111(4)	(15^-)	(14^-)	722.2(4)	1.8(9)	4.6105(3)	3.8883(4)	(19^+)	(17^+)
337.2(2)	4(1)	4.3724(3)	(4.0354(4))	(18^+)		831.6(2)	3.7(8)	1.8536(2)	1.0217(2)	(12^+)	(10^+)
397.5(2)	4(1)	4.7699(3)	4.3724(3)		(18^+)	835.2(1)	9(2)	0.8654(1)	0.0311(3)	(9^+)	(7^+)
406.9(1)	55(9)	1.4285(2)	1.0217(2)	(11^+)	(10^+)	896.5(3)	1.7(5)	4.3724(3)	3.4756(4)	(18^+)	(16^+)
407.8(4)	13(3)	2.2611(4)	1.8536(2)	(14^+)	(12^+)	1214.2(3)	6(2)	3.4756(4)	2.2611(4)	(16^+)	(14^+)
412.8(4)	3(1)	3.8883(4)	3.4756(4)	(17^+)	(16^+)	(892)	–	2.3206(5)	1.4285(2)	(12^-)	(11^+)
425.45(9)	29(5)	1.8536(2)	1.4285(2)	(12^+)	(11^+)	(1030)	–	3.8883(4)	2.8581(5)	(17^+)	(15^+)

(D pair), and four (G pair). Therefore, the collective states in the medium-heavy nuclei are described rather well. In the present work, it is assumed that (i) the ^{132}Sn nucleus is an inert core, (ii) the pair nucleons are in the model space of $\pi(1d_{5/2},0g_{7/2},0h_{11/2})$ and $\nu(2s_{1/2},1d_{3/2},1d_{5/2},0g_{7/2},0h_{11/2})$, and (iii) the unpaired nucleons are in the $h_{11/2}$ orbits. In order to recover the trade-off of the truncation, the non-collective pairs in $\pi(0h_{11/2})$ and $\nu(0h_{11/2})$ are taken into account. The single particle energies of neutrons and protons are taken from the experimental level energies in ^{131}Sn and ^{133}Sb, respectively.

Figure 13 shows the experimental and the theoretical level energies of the $\pi h_{11/2} \otimes \nu h_{11/2}^{-1}$ band members in ^{136}La. It is seen that, except for the 14^+ isomer level, the lower spin states of up to 17^+ are in rather good agreement between the experimental and the PTSM levels. Examining the level spacing, it is noticed that the PTSM predicts the 14^+ level at lower energy than what is expected from the extrapolation from the $I < 14$ levels in the E vs. I plane. However, the experimental 14^+ level lowering is more.

The experimental and calculated kinematic moment of inertia $\mathcal{J}^{(1)}$ defined as

$$\mathcal{J}^{(1)}(I) = \frac{2I-1}{E(I)-E(I-2)} \tag{1}$$

is one of the clues to the nuclear structure. Figure 14 shows $\mathcal{J}^{(1)}$ as a function of spin for the experimental and PTSM results of ^{136}La, together with the experimental values of ^{134}La [18] for comparison. It is found that the experimental $\mathcal{J}^{(1)}$ of ^{134}La shows very small dependence on spin, which means that the structure of this band does not change up to high spin, whereas both the experimental and the theoretical values of ^{136}La show maxima at 14^+, and the experimental data show a rapid increase again after 17^+. It is interesting to note that the PTSM predicts structure change at 14^+, as observed in the lowering of the predicted 14^+ level. The detailed examination of the number of pairs as a function of spin shows (i) a rapid increase of the number of $\pi g_{7/2}$ pairs between 12^+ and 17^+

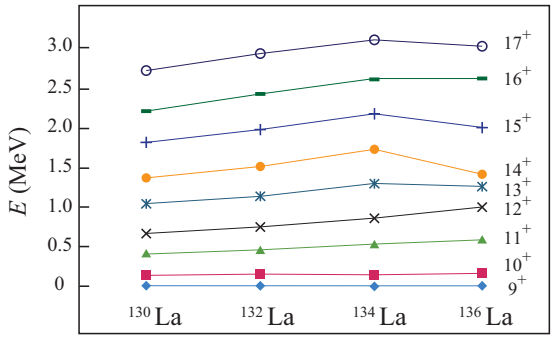

FIG. 11. (Color online) Comparison of the experimental level energies of the $\pi h_{11/2} \otimes \nu h_{11/2}^{-1}$ bands in La isotopes. The level energy is plotted relative to the 9^+ band head.

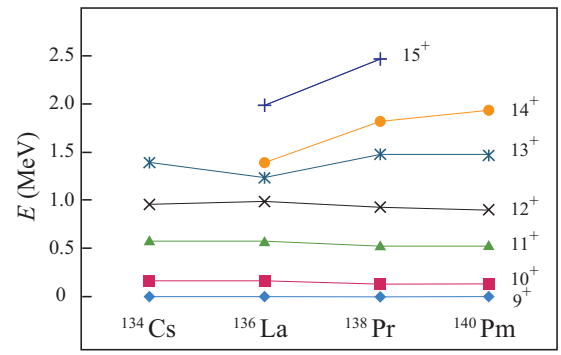

FIG. 12. (Color online) Comparison of the experimental level energies of the $\pi h_{11/2} \otimes \nu h_{11/2}^{-1}$ bands in the $N = 79$ isotones, ^{134}Cs, ^{136}La, ^{138}Pr, and ^{140}Pm. The level energy is plotted relative to the 9^+ band head.

TABLE II. Experimental partial half-lives and Weisskopf estimates of the γ transitions depopulating the (14^+) isomer [$\widetilde{E_x}$ = 2.261 MeV, $T_{1/2}$ = 187(27) ns] in ^{136}La.

E_γ(keV)	Intensity	Partial half-life (ns)	$\sigma\lambda$	$B(\sigma\lambda)$(W.u.)
149	5.4	637	$M1$	1.0×10^{-5}
408	13	265	$E2$	4.5×10^{-3}

and (ii) the largest number of G pairs at 14^+. It is speculated that the increase of the $\pi g_{7/2}$ pairs induces the structure change of the core at the 14^+ level. The experimental data suggest a more significant structure change at 14^+. This must be the reason for the isomerism. The fact that there was found no other isomer at high-spin region suggests that the structure of the levels with spins higher than 14 may be similar to that of the 14^+ isomer.

Although the PTSM predicts the structure change to some extent, it can not reproduce the transition probabilities of the 14^+ isomer: $B(M1)_{\rm exp} = 1.9 \times 10^{-5}$ $[(\mu_N)^2]$ and $B(M1)_{\rm PTSM} = 3.92$ $[(\mu_N)^2]$, $B(E2)_{\rm exp} = 1.9 \times 10^{-5}$ $[(e\text{b})^2]$, and $B(E2)_{\rm PTSM} = 8.25 \times 10^{-3}$ $[(e\text{b})^2]$. This may be improved by extending the model space.

C. Comparison with cranked Nilsson-Strutinsky model prediction

The level structure of ^{136}La was also investigated by the cranked Nilsson-Strutinsky (CNS) model. Although this model does not take into account the paring interactions, it has been successful in predicting various high-spin structures such as shape coexistence, shape change, and band crossing in medium-heavy mass region [25]. In this model, the total energy of a specific spin state is calculated as a coupling of the rotating core and valence particles in a three dimensional space of the deformation parameters ϵ_2, ϵ_4, and γ. The states with the minimum energy most likely correspond to the observed high-spin states.

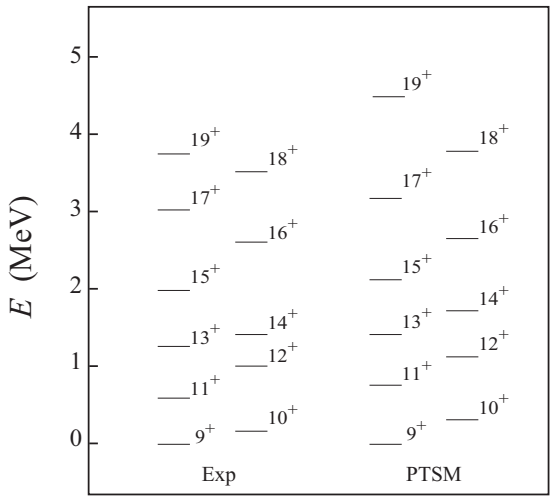

FIG. 13. Comparison of the level energies in ^{136}La between the experimental results and the PTSM predictions. The level energies are rescaled with respect to the 9^+ state.

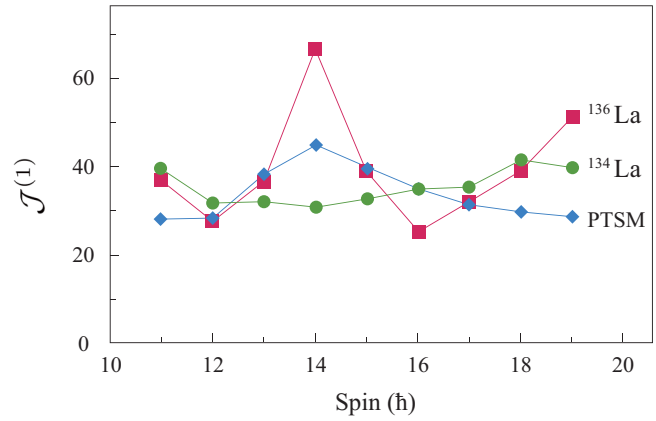

FIG. 14. (Color online) Comparison of the kinematic moment of inertia $\mathcal{J}^{(1)}$ in ^{136}La between the experimental results (square) and the PTSM predictions (diamond), together with the experimental values of ^{134}La (closed circle, data from Ref. [18]).

In ^{136}La, the predicted yrast states with 9^+–13^+ have the $\pi h_{11/2} \otimes \nu h_{11/2}^{-1}$ configuration ($\epsilon_2 \sim 0.15, \gamma \sim 30^\circ$), whereas the 14^+ state has the $\pi(d_{5/2}g_{7/2})^1 \otimes \nu(s_{1/2}d_{3/2}d_{5/2}g_{7/2})^1 h_{11/2}^{-2}$ configuration with very different deformation parameters ($\epsilon_2 \sim 0.10, \gamma \sim -135^\circ$). The higher-spin levels are predicted with similar deformation parameters to those of the 14^+ state. Therefore, the isomerism of the 14^+ state is also explained by the CNS calculations as due to a drastic shape change.

It is suggested that a new type of collective structure is induced by the increase of the number of $\pi g_{7/2}$ pairs and/or by the configuration change associated with the shape change in ^{136}La. From the systematic data of $N = 79$ isotones and La isotopes, similar structure change is expected in ^{134}Cs and ^{138}La.

V. SUMMARY

The high-spin states of the odd-odd nucleus ^{136}La have been investigated by the radioactive-beam-induced fusion-evaporation reaction of ^{124}Sn(^{17}N,5n) at 5.2 MeV/u. The use of radioactive beam enabled an efficient population of the high-spin states in ^{136}La, which is located close to the β-stability line in a nuclear chart. Event-by-event measurements of the time correlation between the beam particles and the in-beam γ rays successfully lead to the finding of a new 14^+ isomer which is located 2.261 MeV above the 114 ms 7^- isomer. The level scheme of ^{136}La has been established by the precise analyses. Most of the level scheme shows rather good agreement with one of the previous three works, except for the 14^+ isomer and new levels at higher excitation-energy region.

The band built on the 9^+ level in ^{136}La shows a typical band structure of the $\pi h_{11/2} \otimes \nu h_{11/2}^{-1}$ band as in the neighboring nuclei. However, the 14^+ isomer in ^{136}La is significantly lower in energy as compared with the 14^+ $\pi h_{11/2} \otimes \nu h_{11/2}^{-1}$ band levels in other La isotopes. Also, the 13^+ and 15^+ levels are lower in a systematics of the $N = 79$ isotones.

The $\pi h_{11/2} \otimes \nu h^{-1}_{11/2}$ band levels in ^{136}La were compared with the pair-truncated shell model (PTSM) calculations, which well reproduce the level structure of the $\pi h_{11/2} \otimes \nu h^{-1}_{11/2}$ bands in ^{132}La and ^{134}La. The PTSM calculations predict the lowering of the 14^+ level in ^{136}La, as is also confirmed in the kinematic moment of inertia $\mathcal{J}^{(1)}$. However, the experimental data show more rapid increase of $\mathcal{J}^{(1)}$ at 14^+ than the PTSM calculations. Also, the PTSM calculations do not reproduce the significantly hindered $14^+ \rightarrow 13^+$ and $14^+ \rightarrow 12^+$ transition probabilities. The existence of the 14^+ isomer suggests the structure change of the core induced by an increase of the number of $\pi g_{7/2}$ pairs.

The isomerism of the 14^+ isomer was also investigated using the cranked Nilsson-Strutinsky (CNS) model, which successfully have explained various high-spin structures in the medium-heavy mass region. In the CNS calculations, a rapid change of the configuration was also predicted at 14^+ when the spin was increased. The calculated nuclear shapes are very different between the states below and above the 14^+ isomer.

The fact that there was found no other isomer at high-spin region suggests that the structure may be similar in levels higher than 14^+. The results of the present work suggest a new type of collective-like structure in the $N = 79$ region. More experimental information on the high-spin states of ^{138}La and ^{134}Cs is needed in order to clarify the mechanism of the structure change in $A = 130$–140 mass region.

ACKNOWLEDGMENTS

The authors are grateful to RCNP, Osaka University for providing with us the intense ^{18}O beam. The authors also acknowledge the IN2P3/EPSRC French/UK loan pool for the loan of germanium detectors. H.N. was supported by JSPS.

[1] E. S. Paul *et al.*, Phys. Rev. Lett. **58**, 984 (1987).
[2] C. M. Petrache *et al.*, Phys. Rev. C **86**, 044321 (2012).
[3] Y. S. Chen, S. Frauendorf, and G. A. Leander, Phys. Rev. C **28**, 2437 (1983).
[4] R. Bengtsson *et al.*, Nucl. Phys. A **415**, 189 (1984).
[5] S. Frauendorf *et al.*, Rev. Mod. Phys. **73**, 463 (2001).
[6] E. W. Cybulska *et al.*, Acta Phys. Pol. B **32**, 929 (2001).
[7] S. J. Zhu *et al.*, Eur. Phys. J. A **24**, 199 (2005).
[8] T. Bhattacharjee *et al.*, Nucl. Phys. A **750**, 199 (2005).
[9] A. A. Sonzogni, Nucl. Data Sheet **95**, 837 (2002).
[10] D. R. Tilley, H. R. Weller, and C. M. Cheves, Nucl. Phys. A **564**, 1 (1993).
[11] F. Pühlhofer, Nucl. Phys. A **280**, 267 (1977).
[12] R. Leguillon *et al.*, Phys. Rev. C **88**, 044309 (2013).
[13] T. Shimoda, H. Miyatake, and S. Morinobu, Nucl. Instrum. Methods Phys. Res. B **70**, 320 (1992).
[14] S. Mitsuoka *et al.*, Nucl. Instrum. Methods Phys. Res. A **372**, 489 (1996).
[15] B. Singh, A. A. Rodionov, and Y. L. Khazov, Nucl. Data Sheet **109**, 517 (2008).
[16] T. Koike, K. Starosta, C. J. Chiara, D. B. Fossan, and D. R. LaFosse, Phys. Rev. C **63**, 061304(R) (2001).
[17] I. Kuti *et al.*, Phys. Rev. C **87**, 044323 (2013).
[18] R. A. Bark *et al.*, Nucl. Phys. A **691**, 577 (2001).
[19] R. S. Hager and E. C. Seltzer, Nucl. Data A **4**, 1 (1968).
[20] H. Pai *et al.*, Phys. Rev. C **84**, 041301(R) (2011).
[21] M. L. Li *et al.*, Phys. Rev. C **75**, 034304 (2007).
[22] J. G. Wang *et al.*, J. Phys. G: Nucl. Part. Phys. **37**, 125107 (2010).
[23] K. Higashiyama, N. Yoshinaga, and K. Tanabe, Phys. Rev. C **72**, 024315 (2005).
[24] K. Higashiyama and N. Yoshinaga, Phys. Rev. C **88**, 034315 (2013).
[25] T. Bengtsson and I. Ragnarsson, Nucl. Phys. A **436**, 14 (1985).